Polarization tunable bidirectional photoresponse in Van der Waals α-In_2Se_3/NbX_2 (X = S, Se, and Te) ferroelectric diodes

Shibo Fang ,[1,*] Qiuhui Li,[1,*] Chen Yang,[1,†] Baochun Wu ,[1,2] Shiqi Liu,[1,3] Jie Yang,[4] Jiachen Ma ,[1,5] Zongmeng Yang,[1] Kechao Tang,[6] and Jing Lu[1,7,8,9,10,‡]

[1]State Key Laboratory for Mesoscopic Physics and School of Physics, Peking University, Beijing 100871, People's Republic of China
[2]State Key Laboratory of Low Dimensional Quantum Physics and Department of Physics, Tsinghua University, Beijing 100871, People's Republic China
[3]Key Laboratory of Spintronics Materials, Devices and Systems of Zhejiang Province, Hangzhou 311305, People's Republic of China
[4]Key Laboratory of Material Physics, School of Physics and Microelectronics, Ministry of Education, Zhengzhou University, Zhengzhou 450001, People's Republic of China
[5]Research Center for Materials, Architectures and Integration of Nanomembranes (MAIN), Chemnitz University of Technology, 09126 Chemnitz, Germany
[6]School of Integrated Circuits, Peking University, Beijing 100871, People's Republic of China
[7]Collaborative Innovation Center of Quantum Matter, Beijing 100871, People's Republic of China
[8]Beijing Key Laboratory for Magnetoelectric Materials and Devices (BKL-MEMD), Peking University, Beijing 100871, People's Republic of China
[9]Peking University Yangtze Delta Institute of Optoelectronics, Nantong 226010, People's Republic of China
[10]Key Laboratory for the Physics and Chemistry of Nanodevices, Peking University, Beijing 100871, People's Republic of China

(Received 10 May 2023; revised 28 July 2023; accepted 7 August 2023; published 28 August 2023)

Ferroelectric diodes can generate a polarization-controlled bidirectional photoresponse to simulate inhibition and promotion behaviors in the artificial neuromorphic system with fast speed, high energy efficiency, and nonvolatility. However, the existing ferroelectric diodes based on ferroelectric oxides suffer from a weak bidirectional photoresponse (below 1 mA/W), difficult miniaturization, and a large response photon energy (over 3 eV). Here, we design a series of van der Waals α-In_2Se_3/NbX_2 (X = S, Se, and Te) ferroelectric diodes with bidirectional photoresponse by using *ab initio* quantum transport simulation. These devices show a maximum bidirectional photoresponse of 30 (−19) mA/W and a minimum response photon energy of 1.3 eV at the monolayer thickness. Our work shows advanced optoelectronic applications of the van der Waals ferroelectric diodes in the future artificial neuromorphic system.

DOI: 10.1103/PhysRevMaterials.7.084412

I. INTRODUCTION

Bidirectional photodetector refers to a device whose photocurrent can switch between different directions when subjected to an outside stimulation [1–3]. In neuromorphic visual systems, a single bidirectional photodetector can represent both positive and negative weights in simulating excitatory and inhibitory behaviors, respectively, which greatly reduces the hardware count in the artificial neural network [4–7]. Existing tunable bidirectional photodetection mainly relies on the gate-controlled band alignment in two-dimensional (2D) materials [2,3] and photothermal effects in metal and semiconductor composite systems [6,8,9]. However, the requirement of the gate-controlled engineering inevitably consumes additional power, and the response time of the photothermal effect is too long [6,8,10].

Ferroelectric diode (Fe diode) is a special kind of diode, whose rectification direction can be switched by the polarization reversal [11–15]. Traditional bulk Fe diode based on ferroelectric oxides can produce nonvolatile symmetrical bidirectional photoresponse by easily switching their electric polarization directions [16]. The switching progress has ultrafast kinetics (<1 ns) and high controllability without a sustaining voltage supply [17]. The switching mechanism originates from the tunable Schottky barrier heights (SBHs) and built-in field modulated by the polarization-induced surface charges [11,13,17,18]. However, the existing ferroelectric-controlled bidirectional photoresponse in the traditional bulk Fe diode has three shortcomings. First, the photoresponse produced by the bulk Fe diode is too low [e.g., 0.05 and 0.22 mA/W in Au/$BiFeO_3$/Au [16] and $Pb(Zr_{0.2}Ti_{0.8})O_3$ Fe diodes [17], respectively] because of their weak interaction with light (the power conversion efficiency reported on most of the ferroelectrics are mostly in the order of 0.5% [19,20]). Second, due to the surface-charge-induced depolarization field, surface crystalline reconstruction, interfacial strain, or weakened dipole-dipole interaction [21–23], the ferroelectricity of the ferroelectric oxide is strongly suppressed in the nanoscale thickness, rendering the device miniaturization difficult [24]. Third, the response photon energy is too large because the band gaps E_g of the ferroelectric

*These authors contributed equally to this work.
†Corresponding author: yangchen96@pku.edu.cn
‡Corresponding author: jinglu@pku.edu.cn

 ©2023 American Physical Society

oxides are mostly over 3 eV [20] (e.g., $E_g = 3.78$ and 5.81 eV for $BaTiO_3$ [25] and c-HfO_2 [26], respectively).

The discovery of 2D van der Waals (vdW) ferroelectric provides a chance to overcome all these shortcomings. First, 2D vdW ferroelectric interacts strongly with light due to the large density of states at the band edges [10,27,28], and its photodetector shows a large responsivity [23,27,29]. Second, the ferroelectricity of the vdW ferroelectric can be maintained down to the monolayer level due to the large atomic displacement [30,31], smooth surface [32], etc. Third, 2D vdW ferroelectric varies from insulators with large band gaps [$E_g = 3.65$ eV in $(C_4NH_3)_2PbCl_4$ [33]] to semimetals without band gap (T_d-WTe_2 [34]), resulting in a wide optoelectronic response range in the vdW Fe diode [32]. Moreover, the ferroelectric-tuned vdW heterojunction can be integrated easily to realize functionality owing to their passivated surfaces and band alignment effect [35,36]. For example, the photocurrent of the α-In_2Se_3/WSe_2 van der Waals heterojunction can be enhanced by about 18 times with applying the tensile strain of 0.433% due to the piezophototronic effect [37]. Among all the room-temperature 2D vdW ferroelectrics, α-In_2Se_3 is very attractive for making the Fe diode because it has not only an ultralow switching electric field (one to two orders of magnitude smaller than the reported values of other 2D vdW ferroelectrics [38]) but also an ultrahigh photoresponse of approximately 10^5 A/W and large detectivities of $(3.3 \pm 0.8)\times 10^{13}$ cm $Hz^{1/2}$/W [39,40]. From a mass production perspective, α-In_2Se_3 has a mature preparation technology that can be synthesized at a large area of centimeter scale with controllable layers [41–43].

In this work, we design a series of vdW α-In_2Se_3/NbX_2 (X = S, Se, and Te) Fe diodes by the density functional theory (DFT) coupled with the nonequilibrium Green's function (NEGF). We reveal a ferroelectric-controlled bistable conduction characteristic and bidirectional photoresponse effect in all the devices (X = S, Se, and Te). The switching mechanism originates from the switching between the p-i junction and the n-i junction. The bidirectional photoresponse shows a maximum symmetrical photoresponse of 30 (−19) mA/W and a minimum response photon energy of 1.3 eV down to the monolayer. Our work reveals a huge potential of the vdW Fe diode in future computing-in-sensor architecture.

II. BILAYER α-In_2Se_3/NbX_2 HETEROJUNCTION

Monolayer α-In_2Se_3 is composed of five covalently bonded monatomic layers in the sequence of Se-In-Se-In-Se, and the atoms in each layer are arranged in a triangular lattice. The optimized lattice constant of α-In_2Se_3 is 4.107 Å. Although the ferroelectricity of monolayer α-In_2Se_3 has not been experimentally confirmed yet, the ferroelectric switching state of few-layer α-In_2Se_3 has been experimentally verified. Besides, the electron microscopy images and the ferroelectric polarization intensity of the few-layer α-In_2Se_3 are in close agreement with theoretical predictions [30,31,41,44]. Due to the low interface effects inherent in van der Waals materials, the existence of ferroelectricity in monolayer α-In_2Se_3 cannot be ruled out. Our study is based on the assumption that the monolayer α-In_2Se_3 exhibits ferroelectricity, serving as the foundation for our research.

When α-In_2Se_3 is in contact with metals, the bands of α-In_2Se_3 undergo a shift due to the combined effects of the electron injection and ferroelectric depolarization field [45–47]. 1H monolayer NbX_2 (X = S, Se, and Te) are vdW metals, consisting of three monatomic layers of X-Nb-X with the calculated lattice constants of 3.35, 3.47, and 3.68 Å, respectively. The work functions of the monolayer NbX_2 are 5.96, 5.82, and 4.85 eV for S, Se, and Te, respectively, and that of the monolayer α-In_2Se_3 is 5.5 eV. The difference of the work functions between α-In_2Se_3 and NbX_2 ranges from 0.32 to 0.65 eV, while the polarization-induced surface band difference of the isolate α-In_2Se_3 reaches 1.41 eV, as shown in Fig. S1(d) of the Supplemental Material [48]. This leads to the dominance of the depolarization field effect, relative to the electron injection effect, on band modulation in the α-In_2Se_3/NbX_2 heterojunction. For example, when the ferroelectric polarization direction of α-In_2Se_3 changes, the Schottky barrier formed at the interfaces with NbX_2 undergoes a transformation between n type and p type [45,46].

The geometries and projected band structures of the α-In_2Se_3/NbX_2 heterostructures are shown in Fig. 1. The supercell of the heterostructure consists of a 2×2 monolayer (ML) NbX_2 and a $\sqrt{3}\times\sqrt{3}$ ML α-In_2Se_3. The in-plane lattice constants of NbX_2 are stretched to match the optimized α-In_2Se_3 lattice constant with mismatches of 1.6−4.3%. Previous works have shown that the electronic properties of the α-In_2Se_3/NbX_2 heterojunction are intact, irrespective of the stacking orders [46]. The α-In_2Se_3/NbX_2 heterojunctions are defined as two states according to different ferroelectric polarization directions, denoted as the P up and down. The P-up state refers to the case where the out-of-plane polarization of α-In_2Se_3 points toward the NbX_2 layer. On the contrary, the P-down state refers to the case where polarization is reversed. The key parameters of the heterostructures, such as layer spacing, binding energy, and SBH, are summarized in Table S1 of the Supplemental Material [48].

Compared with the band structure of the isolated ML α-In_2Se_3, as shown in Fig. S1(a) [48], the projected band structure of the ML α-In_2Se_3 in the α-In_2Se_3/NbX_2 heterojunction is shifted by the depolarization field and electron injection of NbX_2. To evaluate such an effect, we define the ferroelectric band shift (ΔE_{FE}) as the difference between the valence band maximum energy E_{VBM} in the projected α-In_2Se_3 in the heterostructure and E_{VBM} in the isolated ML α-In_2Se_3:

$$\Delta E_{FE} = E_{VBM}(\alpha{-}In_2Se_3/NbX_2) - E_{VBM}(\alpha{-}In_2Se_3). \quad (1)$$

As shown in Table S1 [48], ΔE_{FE} is 0.45, 0.75, and 0.3 eV for the α-In_2Se_3/NbX_2 (X = S, Se, and Te) P-up states, respectively, while ΔE_{FE} is 0.07, −0.05, and −0.35 eV for P-down states, respectively. The positive ΔE_{FE} indicates that the α-In_2Se_3 in the heterostructure is p doped because its E_{VBM} is closer to the Fermi level than that of the intrinsic α-In_2Se_3. On the contrary, the negative ΔE_{FE} corresponds to an n-doped case. When the heterostructure is in the P-up/-down state, the depolarization charge is negative/positive, resulting in the band structure of the α-In_2Se_3 layer being p/n doped, respectively. The depolarization field in the NbX_2 can also be confirmed by the p_z orbital splitting of the α-In_2Se_3

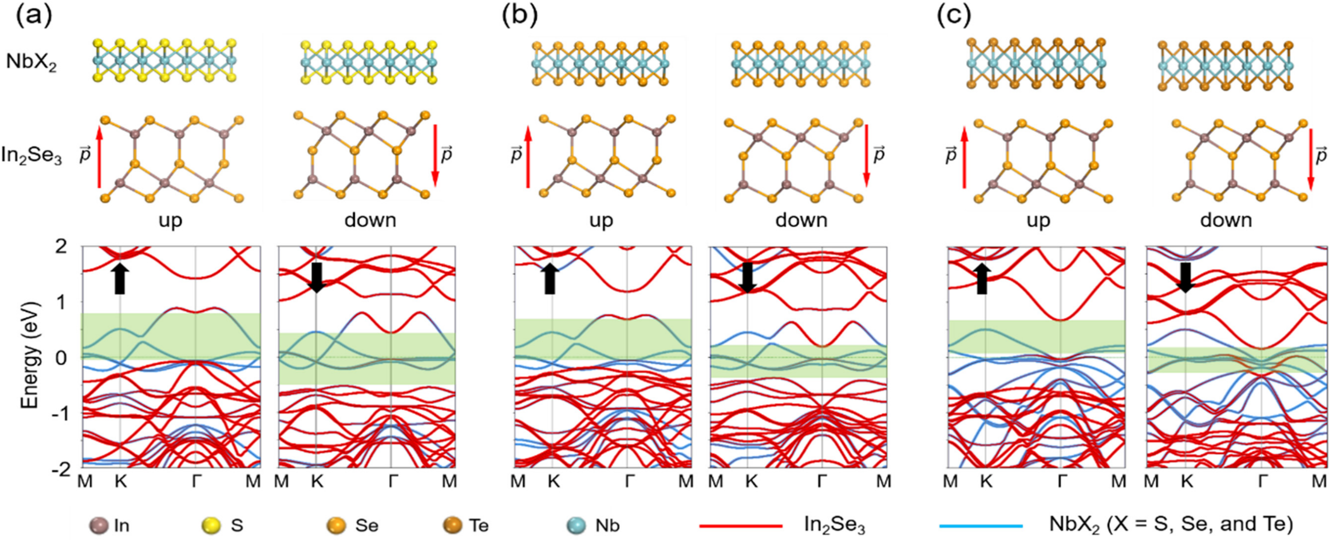

FIG. 1. Geometries and band structures of the bilayer (a) α-In_2Se_3/NbS_2, (b) α-In_2Se_3/$NbSe_2$, and (c) α-In_2Se_3/$NbTe_2$ under different electric polarizations of α-In_2Se_3. The red arrows point to the electric polarization direction of α-In_2Se_3. The black arrows point to the α-In_2Se_3 band shift direction induced by NbX_2. The green transparent area denotes the band-gap region of α-In_2Se_3.

layer and the shielding effective potential in the heterostructure, as shown in Figs. S2 and S3, respectively [48].

III. SWITCHABLE PHOTOCURRENT TRANSPORT PROPERTIES

The vdW α-In_2Se_3/NbX_2 Fe diode is simulated by a two-probe model based on the density-functional theory (DFT) coupled with the nonequilibrium Green's function (NEGF) method, as shown in Fig. 2. The center region is illuminated by the light, and the photocurrent flowing into the left electrode is evaluated. We consider two linear polarized lights. One is along the y axis with a polarizing angle $\theta(e_1 = \cos\theta z + \sin\theta x)$, and the other is along the z axis with a polarizing angle $\varphi(e_2 = \cos\varphi z + \sin\varphi y)$.

The local device density of states projected to the α-In_2Se_3 layer in the α-In_2Se_3/NbX_2 Fe diodes are calculated by *ab initio* quantum transport simulation, as shown in Fig. 3. According to the transport simulation result, $\Delta E_{\rm FEs}$ of the heterostructure in the P-up (down) configuration are 0.3 (−0.25), 0.5 (−0.2), and 0.05 (−0.8) eV for X = S, Se, and Te, respectively. The positive and negative $\Delta E_{\rm FEs}$ indicate that α-In_2Se_3 is p and n doped, respectively. Hence, when the Fe diode is in the P-up state, the α-In_2Se_3 layers in the left electrode and central region are p doped, while α-In_2Se_3 in the right electrode is still intrinsic, resulting in a formation of a p-i junction. As the device is in the P-down state, the left electrode and central region are n doped, and the right electrode is intrinsic, resulting in the formation of an n-i junction.

The photoresponse R (the ratio of the photocurrent to the incident light power, $R = I_{\rm ph}/P_{\rm ph}$, where $I_{\rm ph}$ is the photocurrent and $P_{\rm ph}$ is the incident light power) incidented by the light along the y axis with a e_1 linear-polarized light of polarizing angle $\theta = 0°$, 45°, and 90° is shown in Figs. 4(a)–4(c). When the Fe diode is in the P-up state, the calculated photoresponse R is mostly positive, irrespective of the wavelength and contact metals. When the device is in the P-down state, the photoresponse changes its direction. These devices all show a symmetrical bidirectional photoresponse effect. The maximum R in the P-up state are 25, 32, and 20 mA/W, and the maximum negative R are −18, −19, and −17.5 mA/W for

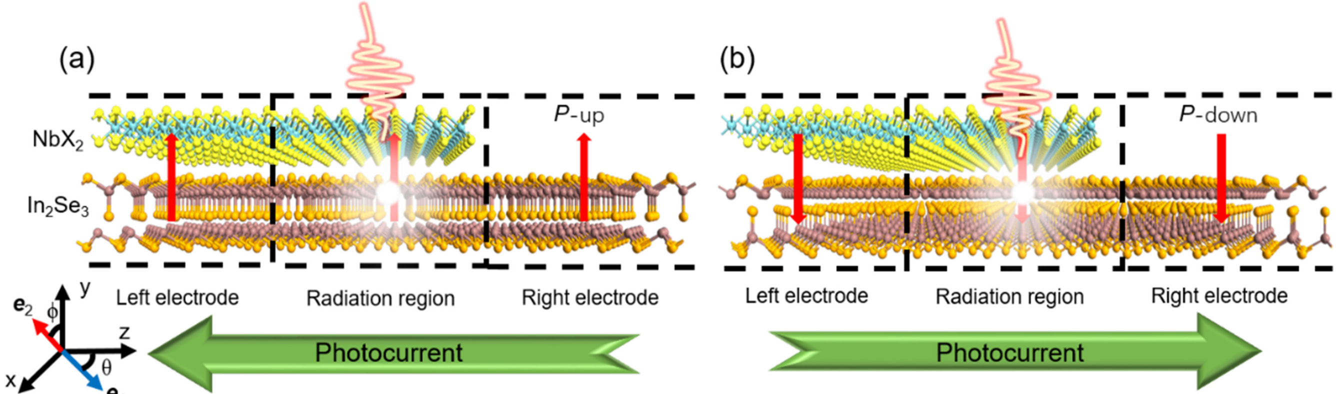

FIG. 2. Fundamental principle of the bidirectional photocurrent in α-In_2Se_3/NbX_2 (X = S, Se, and Te) ferroelectric diode for (a) up and (b) down polarization states.

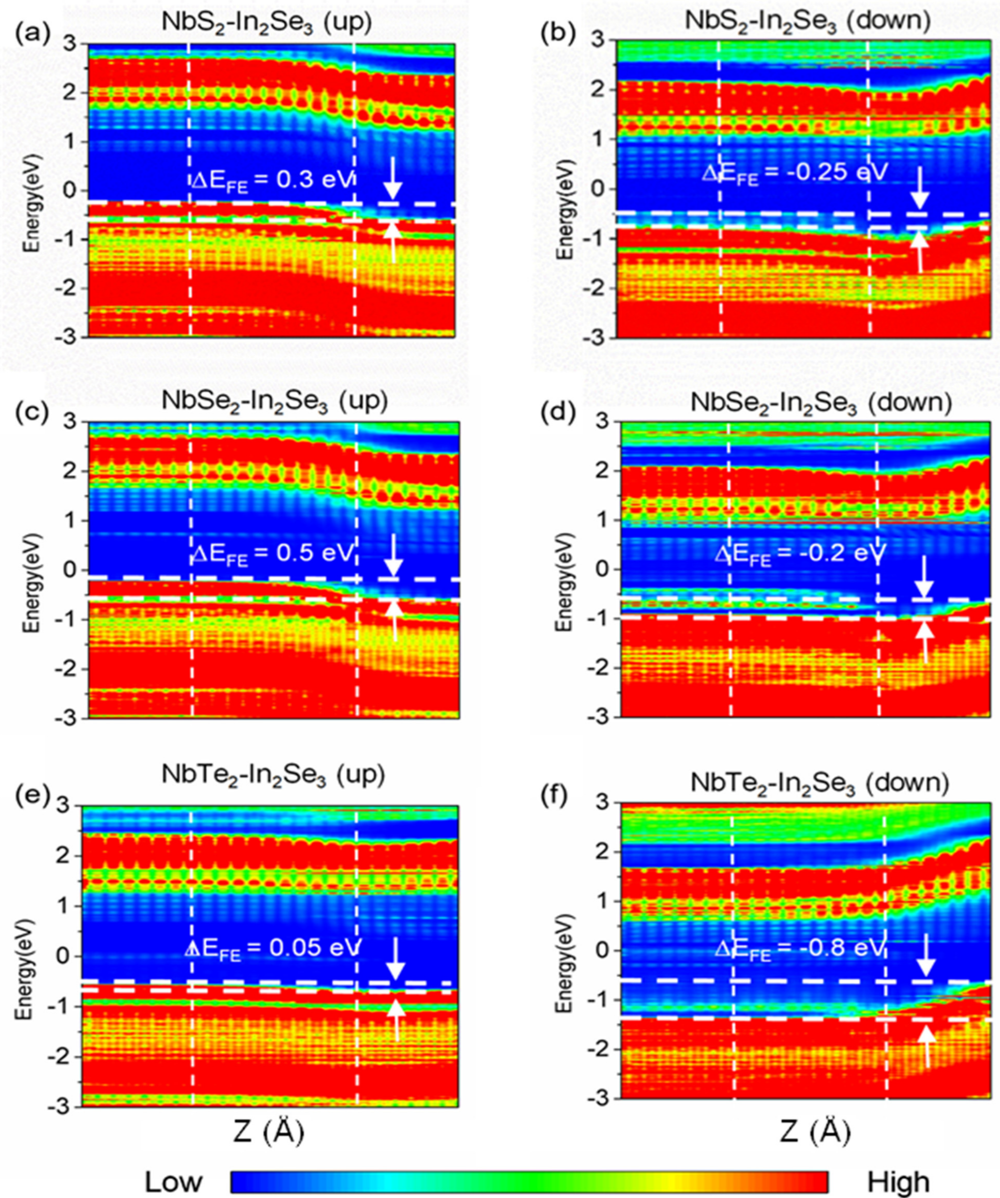

FIG. 3. Local device density of states of the α-In_2Se_3/NbS_2 Fe diode (a) *P*-up configuration and (b) *P*-down configuration. Panels (c) and (e) are same as (a) but for X = Se and Te, respectively. Panels (d) and (f) are same as (b) but for X = Se and Te, respectively. The distance between the two horizontal dashed white lines in each panel represents the ferroelectric band shift (ΔE_{FE}). The central and electrode regions are separated by the vertical white dashed lines.

X = S, Se, and Te, respectively. These values are comparable with the experimental photoresponse of the vdW photodetectors (16.6 mA/W for MoS_2 [60] and 10 mA/W for WSe_2 [29]) and two orders of magnitude larger than that in the bulk $Pb(Zr_{0.2}Ti_{0.8})O_3$ Fe diode [17]. As θ changes from 0° to 90°, R in each device changes slightly, implying these devices are not sensitive to the polarization angle θ. The absorption edges under e_1 polarized light, defined as the minimum absorbed photon energy, of the α-In_2Se_3/NbX_2 (X = S, Se, and Te) Fe diodes are 1.3, 1.2, and 0.9 eV, respectively. The absorption edges are all below the absorbance edge (1.45 eV) of the intrinsic ML α-In_2Se_3 [31], which is attributed to the NbX_2-induced interface gap states.

When the light is incident along the z axis with e_2-polarized linear lights of polarizing angle $\varphi = 0°$, 30°, 60°, and 90°, the symmetrical bidirectional photoresponse effect still holds, as shown in Figs. 4(d)–4(e). This result indicates such bidirectional photoresponse is also not sensitive to the incident light direction. It is worth noting that there are a few abnormal photocurrents that are opposite to their corresponding directions in both *P*-up and -down states. For example, R is supposed to be positive/negative but gives the value of −0.47/3.24 mA/W in the *P*-up/-down states of the NbS_2 device both at $\varphi = 30°$, respectively. Such abnormal photoresponse is attributed to the photogalvanic effect, which is generated from the spatial inversion symmetry breaking and is sensitive to the photon

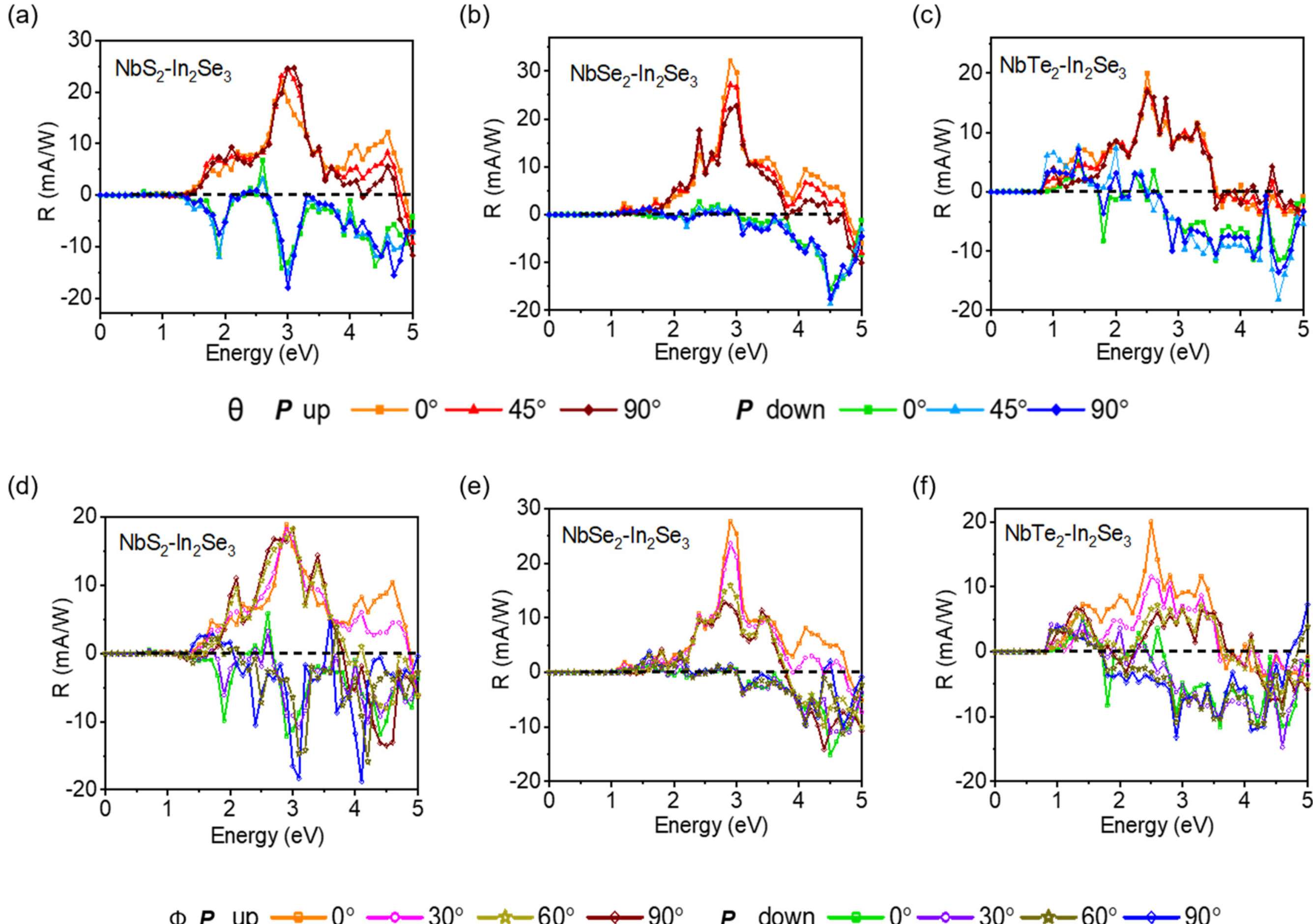

FIG. 4. (a) Photoresponse of the vdW α-In_2Se_3/NbS_2 ferroelectric switchable diode under different ferroelectric polarizations and linear polarized light incident along the y axis with a polaring angle θ. Panels (b) and (c) are same as (a) but for the $NbSe_2$ and $NbTe_2$, respectively. Panel (d) is same as (a) but for the linear polarized light incident along the z axis with the polaring angle Φ. Panels (e) and (f) are same as (d) but for $NbSe_2$ and $NbTe_2$, respectively.

energy and polarizing angle [20,84,85]. Furthermore, there is no photoresponse generated around the Fermi level (E = 0 eV), indicating that the intraband absorbance in the NbX_2 layer is negligible in such devices. We attribute this effect to the fact that there is no direct contact between the right electrode and the NbX_2 layer in the lighting region, resulting in no photocurrent contributed by the NbX_2 layer. The impact of the photogalvanic effect during the polarization switch is shown in Fig. S4 [48]. The result shows that only when the in-place polarization of α-In_2Se_3 is collinear to the transport direction, the bidirectional photoresponse induced by the photogalvanic effect appears. However, in the α-In_2Se_3/NbX_2 Fe diode studied in this paper, the in-plane polarization of α-In_2Se_3 is perpendicular to the transport direction, and thus the directional photoresponse is only contributed by the interface band-bending effect.

IV. DISCUSSION

The electrical transport properties of vdW α-In_2Se_3/NbX_2 Fe diode are simulated in Fig. S5 [48]. The comparison of the biconductance characteristics between the reported Fe diode and this work is listed in Table S2 [48]. Although the maximum on/off ratio (2×10^5%) of the α-In_2Se_3/NbX_2 Fe diodes does not exceed the reported on/off ratio (10^6%) in the $Hf_{0.5}Zr_{0.5}O_2$ Fe diode [15], this value is still larger than most of the on/off ratios in the perovskite and vdW ferroelectric-based Fe diodes [11,13,59,64,86]. The maximum on-state current density (611 mA/mm) of the α-In_2Se_3/$NbTe_2$ Fe diode is comparable with the theoretical on-state currents in the lateral vdW MoS_2 transistors (473 mA/mm by DFT + NEGF [87]). During the simulation, we expect that the switching electric fields E_{switch} of the α-In_2Se_3/$NbSe_2$ Fe diodes should not exceed the lowest reported E_{switch} of 750 kV/cm in the α-In_2Se_3 Fe diodes [50] because the NbX_2 has little impact on the switching barrier of α-In_2Se_3 [46]. Hence, the maximum bias voltage ($|V_{ds}| = 0.4$ V, i.e., E = 600 kV/cm) in this work does not exceed the switching electric field. For future studies, the Fe diode may be improved by placing another NbX_2 electrode below the right α-In_2Se_3 electrode, to unify the rectification direction at both electrodes. Experimentally, the entire device is made of vdW materials, so it is possible to fabricate such vdW Fe diodes by the exfoliation and transfer method [3,32]. The proposed fabrication process flow of the vdW α-In_2Se_3/NbX_2 Fe diode is shown in Fig. S6 [48].

The comparison between the reported bidirectional photoresponse device and this work is listed in Table S3 [48]. Until now, various devices except Fe diodes have been introduced to generate bidirectional photoresponse, such as photothermoelectric, photoelectrochemical, and pyroelectric effects. Most dual-polarity photoresponse based on these mechanisms is sensitive to the wavelength of the light, bias or gate voltage, illumination position, pressure, and solute [1,8]. For example, Wang *et al.* have reported a *p*-AlGaN/*n*-GaN *p*-*n* heterojunction photodetector with the photoresponse of −175 mA/W at 254 nm and 31 mA/W at 365 nm based on the joint effect of the photovoltaic effect and redox reaction [1]. There are also some devices that do not depend on wavelength but require a tedious operation to achieve bidirectional photocurrent. For example, the direction of the photocurrent can be reversibly modulated by tuning the ratio of $PtSe_2$ in the Pt/$PtSe_2$ film, which is ascribed to the synergistic mechanism of the bolometric effect of Pt and photoconductive effect of $PtSe_2$ [6]. By contrast, bidirectional photodetection based on Fe diodes shows convenient adjustability and robust dual-polarity photocurrent, irrespective of the incident light [16,17]. The maximum photoresponse (30 mA/W) in the α-In_2Se_3/NbX_2 Fe diode is much larger than those [0.27 μA/W in $BaTiO_3$ [75], 0.05 mA/W in $BiFeO_3$ [16], and 0.22 mA/W in $Pb(Zr_{0.2}Ti_{0.8})O_3$ [17]] of the bulk Fe diode. In addition, there are other mechanisms where the photocurrent can be controlled by ferroelectricity. These switch mechanisms mainly come from the photogalvanic effect, polarization-induced built-field change, and electron density redistribution [27,38,88,89]. However, none of these devices can achieve such controlled bidirectional photoresponse as the Fe diodes [7,17]. Our theoretical calculations only represent the ideal limits of our configurations and ignore many factors. It is unfair to compare them with the experimental results in other configurations directly. Our intention is to provide readers with a summary of the relevant progress.

V. CONCLUSION

We design a series of vdW α-In_2Se_3/NbX_2 (X = S, Se, and Te) ferroelectric diodes by *ab initio* quantum transport simulation. These devices all show a noteworthy ferroelectric-controlled bistable conduction characteristic and bidirectional photoresponse effect. The switchable effect comes from the polarization-controlled band alignment effect. The maximum positive (negative) photoresponse of the α-In_2Se_3/NbX_2 ferroelectric diodes is symmetrical and reaches values of 25 (−18), 32 (−19), and 20 (−17.5) mA/W for X = S, Se, and Te, respectively. Our work reveals the huge potential of the vdW ferroelectric diode for nonvolatile storage and bidirectional optoelectronics.

ACKNOWLEDGMENTS

This work was supported by the Ministry of Science and Technology of China (Grant No. 2022YFA1203904), the National Natural Science Foundation of China (Grants No. 12274002 and No. 91964101), and the Fundamental Research Funds for the Central Universities of Peking University, and the High-performance Computing Platform of Peking University.

The authors declare no conflict of interest.

[1] D. Wang, X. Liu, Y. Kang, X. Wang, Y. Wu, S. Fang, H. Yu, M. H. Memon, H. Zhang, W. Hu, Z. Mi, L. Fu, H. Sun, and S. Long, Bidirectional photocurrent in p–n heterojunction nanowires, Nat. Electron. **4**, 645 (2021).

[2] Y. Wang, E. Liu, A. Gao, T. Cao, M. Long, C. Pan, L. Zhang, J. Zeng, C. Wang, W. Hu, S. J. Liang, and F. Miao, Negative photoconductance in van der waals heterostructure-based floating gate phototransistor, ACS Nano **12**, 9513 (2018).

[3] S. Ghosh, A. Varghese, H. Jawa, Y. Yin, N. V. Medhekar, and S. Lodha, Polarity-tunable photocurrent through band alignment engineering in a high-speed WSe_2/$SnSe_2$ diode with large negative responsivity, ACS Nano **16**, 4578 (2022).

[4] J. Zhu, T. Zhang, Y. Yang, and R. Huang, A comprehensive review on emerging artificial neuromorphic devices, Appl. Phys. Rev. **7**, 011312 (2020).

[5] Y. X. Hou, Y. Li, Z. C. Zhang, J. Q. Li, D. H. Qi, X. D. Chen, J. J. Wang, B. W. Yao, M. X. Yu, T. B. Lu, and J. Zhang, Large-scale and flexible optical synapses for neuromorphic computing and integrated visible information sensing memory processing, ACS Nano **15**, 1497 (2021).

[6] Y. Lian, J. Han, M. Yang, S. Peng, C. Zhang, C. Han, X. Zhang, X. Liu, H. Zhou, Y. Wang, C. Lan, J. Gou, Y. Jiang, Y. Liao, H. Yu, and J. Wang, Tunable bi-directional photoresponse in hybrid $PtSe_{2-x}$ thin films based on precisely controllable selenization engineering, Adv. Funct. Mater. **32**, 2205709 (2022).

[7] Y. Sun, S. Xu, Z. Xu, J. Tian, M. Bai, Z. Qi, Y. Niu, H. H. Aung, X. Xiong, J. Han, C. Lu, J. Yin, S. Wang, Q. Chen, R. Tenne, A. Zak, and Y. Guo, Mesoscopic sliding ferroelectricity enabled photovoltaic random access memory for material-level artificial vision system, Nat. Commun. **13**, 5391 (2022).

[8] B. Ouyang, Y. Wang, R. Zhang, H. Olin, and Y. Yang, Dual-polarity output response-based photoelectric devices, Cell Rep. Phys. Sci. **2**, 100418 (2021).

[9] J.-Y. Wu, Y. T. Chun, S. Li, T. Zhang, J. Wang, P. K. Shrestha, and D. Chu, Broadband MoS_2 field-effect phototransistors: ultrasensitive visible-light photoresponse and negative infrared photoresponse, Adv. Mater. **30**, 1705880 (2018).

[10] M. Long, P. Wang, H. Fang, and W. Hu, Progress, challenges, and opportunities for 2D material based photodetectors, Adv. Funct. Mater. **29**, 1803807 (2018).

[11] P. W. M. Blom, R. M. Wolf, J. F. M. Cillessen, and M. P. C. M. Krijn, Ferroelectric Schottky Diode, Phys. Rev. Lett. **73**, 2107 (1994).

[12] S. L. T. Choi, Y. J. Choi, V. Kiryukhin, and S.-W. Cheong, Switchable ferroelectric diode and photovoltaic effect in $BiFeO_3$, Science **324**, 63 (2009).

[13] C. Wang, K.-J. Jin, Z.-T. Xu, L. Wang, C. Ge, H.-B. Lu, H.-Z. Guo, M. He, and G.-Z. Yang, Switchable diode effect and ferroelectric resistive switching in epitaxial $BiFeO_3$ thin films, Appl. Phys. Lett. **98**, 192901 (2011).

[14] H. Wang, Z. R. Liu, H. Y. Yoong, T. R. Paudel, J. X. Xiao, R. Guo, W. N. Lin, P. Yang, J. Wang, G. M. Chow, T. Venkatesan, E. Y. Tsymbal, H. Tian, and J. S. Chen, Direct observation of room-temperature out-of-plane ferroelectricity and tunneling

electroresistance at the two-dimensional limit, Nat. Commun. **9**, 3319 (2018).
[15] Q. Luo, Y. Cheng, J. Yang, R. Cao, H. Ma, Y. Yang, R. Huang, W. Wei, Y. Zheng, T. Gong, J. Yu, X. Xu, P. Yuan, X. Li, L. Tai, H. Yu, D. Shang, Q. Liu, B. Yu, Q. Ren, H. Lv, and M. Liu, A highly CMOS compatible hafnia-based ferroelectric diode, Nat. Commun. **11**, 1391 (2020).
[16] H. T. Yi, T. Choi, S. G. Choi, Y. S. Oh, and S. W. Cheong, Mechanism of the switchable photovoltaic effect in ferroelectric $BiFeO_3$, Adv. Mater. **23**, 3403 (2011).
[17] B. Cui, Z. Fan, W. Li, Y. Chen, S. Dong, Z. Tan, S. Cheng, B. Tian, R. Tao, G. Tian, D. Chen, Z. Hou, M. Qin, M. Zeng, X. Lu, G. Zhou, X. Gao, and J. M. Liu, Ferroelectric photosensor network: An advanced hardware solution to real-time machine vision, Nat. Commun. **13**, 1707 (2022).
[18] A. K. Saha, M. Si, P. D. Ye, and S. K. Gupta, α-In_2Se_3 based ferroelectric-semiconductor metal junction for non-volatile memories, Appl. Phys. Lett. **117**, 183504 (2020).
[19] Y. Yuan, Z. Xiao, B. Yang, and J. Huang, Arising applications of ferroelectric materials in photovoltaic devices, J. Mater. Chem. A **2**, 6027 (2014).
[20] S. Pal, N. V. Sarath, K. S. Priya, and P. Murugavel, A review on ferroelectric systems for next generation photovoltaic applications, J. Phys. D: Appl. Phys. **55**, 283001 (2022).
[21] H. Sun, J. Gu, Y. Li, T. R. Paudel, D. Liu, J. Wang, Y. Zang, C. Gu, J. Yang, W. Sun, Z. Gu, E. Y. Tsymbal, J. Liu, H. Huang, D. Wu, and Y. Nie, Prominent Size Effects without a Depolarization Field Observed in Ultrathin Ferroelectric Oxide Membranes, Phys. Rev. Lett. **130**, 126801 (2023).
[22] T. Jin, J. Mao, J. Gao, C. Han, K. P. Loh, A. T. S. Wee, and W. Chen, Ferroelectrics-integrated two-dimensional devices toward next-generation electronics, ACS Nano **16**, 13595 (2022).
[23] L. Qi, S. Ruan, and Y. J. Zeng, Review on recent developments in 2D ferroelectrics: Theories and applications, Adv. Mater. **33**, e2005098 (2021).
[24] M. Wu, 100 years of ferroelectricity, Nat. Rev. Phys. **3**, 726 (2021).
[25] R. Fei, L. Z. Tan, and A. M. Rappe, Shift-current bulk photovoltaic effect influenced by quasiparticle and exciton, Phys. Rev. B **101**, 045104 (2020).
[26] R. Kumar, R. Kumar, A. Vij, and M. Singh, A first-principle study of electronic, thermoelectric, and optical properties of sulfur doped c-HfO_2, Phys. Scr. **97**, 075813 (2022).
[27] S. Fang, C. Yang, Q. Li, B. Wu, L. Xu, S. Liu, J. Yang, J. Ma, J. Dong, Y. Li, J. Yang, and J. Lu, Ferroelectric-Tunable Photoresponse in α-In_2Se_3 Photovoltaic Photodetectors: An *Ab Initio* Quantum Transport Study, Phys. Rev. Appl. **19**, 024024 (2023).
[28] H. Tang, B. Shi, Y. Wang, C. Yang, S. Liu, Y. Li, R. Quhe, and J. Lu, Layer-Dependent Photoabsorption and Photovoltaic Effects in Two-Dimensional Bi_2O_2X (X = S, Se, and Te), Phys. Rev. Appl. **15**, 064037 (2021).
[29] A. Pospischil, M. M. Furchi, and T. Mueller, Solar-energy conversion and light emission in an atomic monolayer p-n diode, Nat. Nanotechnol. **9**, 257 (2014).
[30] J. Xiao, H. Zhu, Y. Wang, W. Feng, Y. Hu, A. Dasgupta, Y. Han, Y. Wang, D. A. Muller, L. W. Martin, P. Hu, and X. Zhang, Intrinsic Two-Dimensional Ferroelectricity with Dipole Locking, Phys. Rev. Lett. **120**, 227601 (2018).
[31] W. Ding, J. Zhu, Z. Wang, Y. Gao, D. Xiao, Y. Gu, Z. Zhang, and W. Zhu, Prediction of intrinsic two-dimensional ferroelectrics in In_2Se_3 and other III_2-VI_3 van der Waals materials, Nat. Commun. **8**, 14956 (2017).
[32] C. Wang, L. You, D. Cobden, and J. Wang, Towards two-dimensional van der Waals ferroelectrics, Nat. Mater. **22**, 542 (2023).
[33] L. You, F. Liu, H. Li, Y. Hu, S. Zhou, L. Chang, Y. Zhou, Q. Fu, G. Yuan, S. Dong, H. J. Fan, A. Gruverman, Z. Liu, and J. Wang, In-plane ferroelectricity in thin flakes of van der waals hybrid perovskite, Adv. Mater. **30**, e1803249 (2018).
[34] Z. Fei, W. Zhao, T. A. Palomaki, B. Sun, M. K. Miller, Z. Zhao, J. Yan, X. Xu, and D. H. Cobden, Ferroelectric switching of a two-dimensional metal, Nature (London) **560**, 336 (2018).
[35] C. Chang, W. Chen, Y. Chen, Y. Chen, Y. Chen, F. Ding, C. Fan, H. Jin Fan, Z. Fan, C. Gong, Y. Gong, Q. He, X. Hong, S. Hu, W. Hu, W. Huang, Y. Huang, W. Ji, D. Li, L.-J. Li *et al.*, Recent progress on two-dimensional materials, Acta Phys. Chim. Sin. **37**, 2108017 (2021).
[36] Y. Chen, X. Wang, L. Huang, X. Wang, W. Jiang, Z. Wang, P. Wang, B. Wu, T. Lin, H. Shen, Z. Wei, W. Hu, X. Meng, J. Chu, and J. Wang, Ferroelectric-tuned van der Waals heterojunction with band alignment evolution, Nat. Commun. **12**, 4030 (2021).
[37] Y. Zhao, F. Guo, R. Ding, W. F. Io, S. Y. Pang, W. Wu, and J. Hao, Piezo-phototronic effect in 2D α-In_2Se_3/WSe_2 van der Waals heterostructure for photodetector with enhanced photoresponse, Adv. Opt. Mater. **9**, 2100864 (2021).
[38] B. Lv, W. Xue, Z. Yan, R. Yang, H. Wu, P. Wang, Y. Zhang, J. Hou, W. Zhu, and X. Xu, Control of photocurrent and multi-state memory by polar order engineering in 2H-stacked α-In_2Se_3 ferroelectric, Sci. China Mater. **65**, 1639 (2022).
[39] J. O. Island, S. I. Blanter, M. Buscema, H. S. van der Zant, and A. Castellanos-Gomez, Gate controlled photocurrent generation mechanisms in high-gain In_2Se_3 phototransistors, Nano Lett. **15**, 7853 (2015).
[40] Y. T. Huang, N. K. Chen, Z. Z. Li, X. P. Wang, H. B. Sun, S. Zhang, and X. B. Li, Two-dimensional In_2Se_3: A rising advanced material for ferroelectric data storage, InfoMat **4**, e12341 (2022).
[41] W. Han, X. Zheng, K. Yang, C. S. Tsang, F. Zheng, L. W. Wong, K. H. Lai, T. Yang, Q. Wei, M. Li, W. F. Io, F. Guo, Y. Cai, N. Wang, J. Hao, S. P. Lau, C. S. Lee, T. H. Ly, M. Yang, and J. Zhao, Phase-controllable large-area two-dimensional In_2Se_3 and ferroelectric heterophase junction, Nat. Nanotechnol. **18**, 55 (2023).
[42] B. Lv, Z. Yan, W. Xue, R. Yang, J. Li, W. Ci, R. Pang, P. Zhou, G. Liu, Z. Liu, W. Zhu, and X. Xu, Layer-dependent ferroelectricity in 2H-stacked few-layer α-In_2Se_3, Mater. Horiz. **8**, 1472 (2021).
[43] Q. He, Z. Tang, M. Dai, H. Shan, H. Yang, Y. Zhang, and X. Luo, epitaxial growth of large area two-dimensional ferroelectric α-In_2Se_3, Nano Lett. **23**, 3098 (2023).
[44] J. Yang, J. Zhou, J. Lu, Z. Luo, J. Yang, and L. Shen, Giant tunnelling electroresistance through 2D sliding ferroelectric materials, Mater. Horiz. **9**, 1422 (2022).
[45] Z. Wang and W. Zhu, tunable band alignments in 2D ferroelectric α-In_2Se_3 based Van der Waals heterostructures, ACS Appl. Electron. Mater. **3**, 5114 (2021).

[46] H. Su, T. Hu, F. Wu, and E. Kan, Controllable vdW contacts between the ferroelectric In_2Se_3 monolayer and two-dimensional metals, J. Phys. Chem. C **125**, 10738 (2021).

[47] C. Yang, X. Zhang, X. Sun, H. Zhang, H. Tang, B. Shi, H. Pang, L. Xu, S. Liu, J. Yang, J. Yan, L. Xu, Z. Zhang, J. Yang, D. Yu, and J. Lu, Planar direction-dependent interfacial properties in monolayer In_2Se_3–metal contacts, Phys. Status Solidi B **257**, 1900198 (2019).

[48] See Supplemental Material at http://link.aps.org/supplemental/10.1103/PhysRevMaterials.7.084412 for computational details; atomic structures, projected band structure, density of states, polarization, and effective potential of the ML α-In_2Se_3; geometry and band structure of monolayer NbX_2 (X = S, Se, and Te); projected density of states, electronic density, and effective potential of the α-In_2Se_3/NbX_2 heterojunction; key parameters of the α-In_2Se_3/NbX_2 heterojunction; the impact of photogalvanic effect during the polarization switch in the isolated α-In_2Se_3 photodetector; proposed fabrication process flow of the α-In_2Se_3/NbX_2 ferroelectric diode; and comparison between the reported ferroelectric switchable diodes and bidirection photocurrent devices with this work. The Supplemental Material also contains Refs. [1,3,6,9,12,13,15–17,27,28,45,49–83].

[49] Q. Li, C. Yang, L. Xu, S. Liu, S. Fang, L. Xu, J. Yang, J. Ma, Y. Li, B. Wu, R. Quhe, K. Tang, and J. Lu, symmetric and excellent scaling behavior in ultrathin n- and p-type gate-all-around inas nanowire transistors, Adv. Funct. Mater. **33**, 2214653 (2023).

[50] Y. Zhang, L. Wang, H. Chen, T. Ma, X. Lu, and K. P. Loh, Analog and digital mode α-In_2Se_3 memristive devices for neuromorphic and memory applications, Adv. Electron. Mater. **7**, 2100609 (2021).

[51] Y. Wang, Y. Zhu, Y. Li, Y. Zhang, D. Yang, and X. Pi, Dual-modal optoelectronic synaptic devices with versatile synaptic plasticity, Adv. Funct. Mater. **32**, 2107973 (2021).

[52] Y. Wang, S. Liu, Q. Li, R. Quhe, C. Yang, Y. Guo, X. Zhang, Y. Pan, J. Li, H. Zhang, L. Xu, B. Shi, H. Tang, Y. Li, J. Yang, Z. Zhang, L. Xiao, F. Pan, and J. Lu, Schottky barrier heights in two-dimensional field-effect transistors: From theory to experiment, Rep. Prog. Phys. **84**, 056501 (2021).

[53] R. Quhe, L. Xu, S. Liu, C. Yang, Y. Wang, H. Li, J. Yang, Q. Li, B. Shi, Y. Li, Y. Pan, X. Sun, J. Li, M. Weng, H. Zhang, Y. Guo, L. Xu, H. Tang, J. Dong, J. Yang, Z. Zhang, M. Lei, F. Pan, and J. Lu, Sub-10 nm two-dimensional transistors: Theory and experiment, Phys. Rep. **938**, 1 (2021).

[54] S. Smidstrup, T. Markussen, P. Vancraeyveld, J. Wellendorff, J. Schneider, T. Gunst, B. Verstichel, D. Stradi, P. A. Khomyakov, U. G. Vej-Hansen, M. E. Lee, S. T. Chill, F. Rasmussen, G. Penazzi, F. Corsetti, A. Ojanpera, K. Jensen, M. L. N. Palsgaard, U. Martinez, A. Blom, M. Brandbyge, and K. Stokbro, QuantumATK: An integrated platform of electronic and atomic-scale modelling tools, J. Phys.: Condens. Matter **32**, 015901 (2020).

[55] S. D. B. Pradhan, J. Li, F. Chowdhury, J. Cherusseri, D. Pandey, D. Dev, A. Krishnaprasad, E. Barrios, A. Towers, A. Gesquiere, L. Tetard, T. Roy, and J. Thomas, Ultrasensitive and ultrathin phototransistors and photonic synapses using perovskite quantum dots grown from graphene lattice, Sci. Adv. **6**, eaay5225 (2020).

[56] R. Quhe, J. Liu, J. Wu, J. Yang, Y. Wang, Q. Li, T. Li, Y. Guo, J. Yang, H. Peng, M. Lei, and J. Lu, High-performance sub-10 nm monolayer Bi_2O_2Se transistors, Nanoscale **11**, 532 (2019).

[57] X. Luo, B. Wang, W. Lv, Y. Wang, W. Lv, Z. Wei, Y. Lu, Z. Liu, Z. Lu, R. Xiong, and Z. Zeng, Multifunctional photodetectors based on nanolayered black phosphorus/$SnS_{0.5}Se_{1.5}$ heterostructures, ACS Appl. Nano Mater. **2**, 3548 (2019).

[58] J. Buckeridge and D. O. Scanlon, Electronic band structure and optical properties of boron arsenide, Phys. Rev. Mater. **3**, 051601(R) (2019).

[59] S. Wan, Y. Li, W. Li, X. Mao, W. Zhu, and H. Zeng, Room-temperature ferroelectricity and a switchable diode effect in two-dimensional α-In_2Se_3 thin layers, Nanoscale **10**, 14885 (2018).

[60] Y. Liu, J. Guo, E. Zhu, L. Liao, S. J. Lee, M. Ding, I. Shakir, V. Gambin, Y. Huang, and X. Duan, Approaching the Schottky-Mott limit in van der Waals metal-semiconductor junctions, Nature (London) **557**, 696 (2018).

[61] J. Chen, L. Zhang, L. Zhang, X. Zheng, L. Xiao, S. Jia, and J. Wang, Photogalvanic effect induced fully spin polarized current and pure spin current in zigzag SiC nanoribbons, Phys. Chem. Chem. Phys. **20**, 26744 (2018).

[62] Y. Wang, P. Huang, M. Ye, R. Quhe, Y. Pan, H. Zhang, H. Zhong, J. Shi, and J. Lu, Many-body effect, carrier mobility, and device performance of hexagonal arsenene and antimonene, Chem. Mater. **29**, 2191 (2017).

[63] Y. Liu, Y. Cai, G. Zhang, Y.-W. Zhang, and K.-W. Ang, Al-doped black phosphorus p-n homojunction diode for high performance photovoltaic, Adv. Funct. Mater. **27**, 1604638 (2017).

[64] F. Liu, L. You, K. L. Seyler, X. Li, P. Yu, J. Lin, X. Wang, J. Zhou, H. Wang, H. He, S. T. Pantelides, W. Zhou, P. Sharma, X. Xu, P. M. Ajayan, J. Wang, and Z. Liu, Room-temperature ferroelectricity in $CuInP_2S_6$ ultrathin flakes, Nat. Commun. **7**, 12357 (2016).

[65] Y. Liang and L. Yang, Carrier Plasmon Induced Nonlinear Band Gap Renormalization in Two-Dimensional Semiconductors, Phys. Rev. Lett. **114**, 063001 (2015).

[66] L. Zhang, K. Gong, J. Chen, L. Liu, Y. Zhu, D. Xiao, and H. Guo, Generation and transport of valley-polarized current in transition-metal dichalcogenides, Phys. Rev. B **90**, 195428 (2014).

[67] M. M. Ugeda, A. J. Bradley, S. F. Shi, F. H. da Jornada, Y. Zhang, D. Y. Qiu, W. Ruan, S. K. Mo, Z. Hussain, Z. X. Shen, F. Wang, S. G. Louie, and M. F. Crommie, Giant bandgap renormalization and excitonic effects in a monolayer transition metal dichalcogenide semiconductor, Nat. Mater. **13**, 1091 (2014).

[68] H. Shi, H. Pan, Y.-W. Zhang, and B. I. Yakobson, Quasiparticle band structures and optical properties of strained monolayer MoS_2 and WS_2, Phys. Rev. B **87**, 155304 (2013).

[69] J. Chen, Y. Hu, and H. Guo, First-principles analysis of photocurrent in graphene P N junctions, Phys. Rev. B **85**, 155441 (2012).

[70] G. Luo, X. Qian, H. Liu, R. Qin, J. Zhou, L. Li, Z. Gao, E. Wang, W.-N. Mei, J. Lu, Y. Li, and S. Nagase, Quasiparticle energies and excitonic effects of the two-dimensional carbon allotrope graphdiyne: Theory and experiment, Phys. Rev. B **84**, 075439 (2011).

[71] S. Grimme, J. Antony, S. Ehrlich, and H. Krieg, A consistent and accurate *ab initio* parametrization of density functional dispersion correction (DFT-D) for the 94 elements H-Pu, J. Chem. Phys. **132**, 154104 (2010).

[72] N. Sai, A. M. Kolpak, and A. M. Rappe, Ferroelectricity in ultrathin perovskite films, Phys. Rev. B **72**, 020101(R) (2005).

[73] M. Brandbyge, J.-L. Mozos, P. Ordejón, J. Taylor, and K. Stokbro, Density-functional method for nonequilibrium electron transport, Phys. Rev. B **65**, 165401 (2002).

[74] J. Taylor, H. Guo, and J. Wang, *Ab initio* modeling of quantum transport properties of molecular electronic devices, Phys. Rev. B **63**, 245407 (2001).

[75] Y. S. Yang, S. J. Lee, S. Yi, B. G. Chae, S. H. Lee, H. J. Joo, and M. S. Jang, Schottky barrier effects in the photocurrent of sol–gel derived lead zirconate titanate thin film capacitors, Appl. Phys. Lett. **76**, 774 (2000).

[76] G. Kresse and D. Joubert, From ultrasoft pseudopotentials to the projector augmented-wave method, Phys. Rev. B **59**, 1758 (1999).

[77] F. Aryasetiawan and O. Gunnarsson, The GW method, Rep. Prog. Phys. **61**, 237 (1998).

[78] J. P. Perdew, K. Burke, and M. Ernzerhof, Generalized Gradient Approximation Made Simple, Phys. Rev. Lett. **77**, 3865 (1996).

[79] W. L. Zhong, Y. G. Wang, P. L. Zhang, and B. D. Qu, Phenomenological study of the size effect on phase transitions in ferroelectric particles, Phys. Rev. B **50**, 698 (1994).

[80] P. E. Blöchl, Projector augmented-wave method, Phys. Rev. B **50**, 17953 (1994).

[81] G. Kresse and J. Hafner, *Ab initio* molecular dynamics for open-shell transition metals, Phys. Rev. B **48**, 13115 (1993).

[82] L. Kleinman and D. M. Bylander, Efficacious Form for Model Pseudopotentials, Phys. Rev. Lett. **48**, 1425 (1982).

[83] H. J. Monkhorst and J. D. Pack, Special points for Brillouin-zone integrations, Phys. Rev. B **13**, 5188 (1976).

[84] C. Paillard, X. Bai, I. C. Infante, M. Guennou, G. Geneste, M. Alexe, J. Kreisel, and B. Dkhil, Photovoltaics with Ferroelectrics: Current Status and Beyond, Adv. Mater. **28**, 5153 (2016).

[85] B. I. Sturman, Ballistic and shift currents in the bulk photovoltaic effect theory, Phys. Usp. **63**, 407 (2020).

[86] S. Y. Yang, L. W. Martin, S. J. Byrnes, T. E. Conry, S. R. Basu, D. Paran, L. Reichertz, J. Ihlefeld, C. Adamo, A. Melville, Y. H. Chu, C. H. Yang, J. L. Musfeldt, D. G. Schlom, J. W. Ager, and R. Ramesh, Photovoltaic effects in $BiFeO_3$, Appl. Phys. Lett. **95**, 062909 (2009).

[87] H. Zhang, B. Shi, L. Xu, J. Yan, W. Zhao, Z. Zhang, Z. Zhang, and J. Lu, Sub-5 nm monolayer MoS_2 transistors toward low-power devices, ACS Appl. Electron. Mater. **3**, 1560 (2021).

[88] Y. Wang, F. Wang, Z. Wang, J. Wang, J. Yang, Y. Yao, N. Li, M. G. Sendeku, X. Zhan, C. Shan, and J. He, Reconfigurable photovoltaic effect for optoelectronic artificial synapse based on ferroelectric p-n junction, Nano Res. **14**, 4328 (2021).

[89] Y. Yang, L. Zhang, J. Chen, X. Zheng, L. Zhang, L. Xiao, and S. Jia, An electrically switchable anti-ferroelectric bilayer In_2Se_3 based opto-spintronic device, Nanoscale **13**, 8555 (2021).